Numerical simulation of Al_2O_3-isopropanol nanofluid flows in tubes of circular cross-section

Pedro Romão
pedro.romao@tecnico.ulisboa.pt

Instituto Superior Técnico, Universidade de Lisboa, Portugal

July 2019

Abstract

The development of more advanced technology with increased cooling needs and the continuous search for solutions with better energetic performances has been motivating the heat transfer community to find alternatives to the cooling techniques employed until now. Such intensive search promoted the advent of nanofluids, a novel type of coolants which is no more than a colloidal suspension of solid nanoparticles into common cooling fluids. The potential exhibited by nanofluids motivated an experimental study regarding the evaluation of the heat transfer performance and the hydrodynamic characteristics of an Al_2O_3-isopropanol nanofluid flow. As a complement, a numerical investigation based on a single-phase conventional approach was proposed, which has resulted in the present work. This study consists in a direct comparison of the measured data with their numerical predictions, which presumes a verification of the validity of the assumptions took to simulate a nanofluid behaving as a homogeneous fluid. Also a parametric analysis testing the influence of each controlling parameter considered in the experiments was conducted to, finally, show and conclude about the influence of the comparison basis on the interpretation of results. As main conclusions, we can state the good agreement between experimental data and predictions for laminar flow. In turbulent flow conditions, the match between predictions and experiments was not so high as for laminar flow, still does not compromise the validity of the assumptions followed. The parametric analysis showed a small increase of the heat transfer coefficient with the addition of nanoparticles for laminar flow and a considerable deterioration in turbulent flow conditions, when compared under a constant mass flow rate condition. The same results interpreted in a constant *Re* basis produced significantly different conclusions, being its use not recommended.

Keywords: Nanofluids, Al_2O_3-isopropanol, Numerical investigation, Single-phase conventional approach, Comparative study

1. Introduction

Improving the efficiencies of thermal equipments means a huge reduction on energy consumption worldwide [1]. As more powerful technology is released, with increased cooling needs and more restricted size constraints, the search for new cooling techniques received much attention from the heat transfer community.

One of them is the use of nanofluids, colloidal supensions of solid nanoparticles into common coolants (usually oxides with dimensions smaller than 100nm), that triggered the attention because of their altered thermal properties, namely its improved thermal conductivity, which was seen to promote the heat transfer capacity in comparison to the respective base fluid [2]. Until now, the mechanisms behind this enhancement were not clearly identified, and no general theory was universally accepted too, reason why the most reliable way to acquire the thermal properties of a nanofluid is effectively measuring them [2].

Despite the importance of thermal conductivity, the parameter responsible to quantify any enhancement on the thermal performance and justify their use over regular fluids is the convective heat transfer coefficient (CHTC). Since it is directly related to the heat transfer rate, its improvement could be the key for the reduction of equipments size and weight, better efficiencies and improved capacity to deal with higher thermal loads [2]. However, this improvement has a cost associated, which is the extra power required to pump a more viscous fluid after the addition of nanoparticles. Any possible study regarding the benefit of using nanofluids should take into account these two important parameters [3].

Comparison between CHTC of nanofluids with those of their base fluids is what will dictate if the use of nanofluids is really valuable or not. Never-

theless, one should carefully consider which comparison basis will he use and be aware of the risks of that choice. An example is conclude about it via constant Reynolds number (Re) comparison basis, as all teams mentioned below did. Keeping Re constant, we are actually comparing two flows at different velocities and completely ignoring the penalty in pumping power due to the addition of nanoparticles. We are mixing contributions from different velocities and thermal properties, so the physical conditions are not the same and they should not be compared. The same happens when computing the Nusselt number (Nu) to evaluate the thermal performance instead of the CHTC, since we are accounting indirectly the influence of the thermal conductivity [3].

Therefore, many teams published works focusing on the experimental evaluation of the CHTC in both laminar and turbulent flow regimes. The majority reported enhancements on CHTC, as the case of [4, 5] for laminar flow and [6, 7] for turbulent flow, especially with the increase of Re and nanoparticle concentration. However, some controversy was brought to the debate with other authors reporting not so auspicious results, like [8].

But not only experimental investigations were carried out regarding nanofluids. Several numerical studies are also reported on the literature using Computational Fluid Dynamics (CFD) techniques [9–11]. Despite being a mixture of fluid and solid particles, in the absence of a general theory the easiest way to model a nanofluid is to assume its behavior similar to a homogeneous fluid with effective thermal properties. This is the so-called single-phase conventional approach and is supported by two main assumptions. As the particles are usually very tiny and in low quantities, they are presumed efficiently mixed with the surrounding fluid. This holds up the first assumption, which states that no slip velocity exists among solid and fluid particles. The other assumption is to consider that both phases co-exist in thermal equilibrium conditions [12]. These computational studies allowed essentially to confirm the evolution trends seen for experimental ones, and to prove that no great difference was verified when comparing single-phase with more complex representations of nanofluid flows.

Although some conclusions presented in common, poor agreement was found between the predictions from regular fluid equations and experimental values in the analyzed papers. This fact goes against what is expected since if it would be possible to consider a nanofluid a homogeneous fluid, the equations developed for classic fluids should be able to predict the nanofluid behavior too. To investigate this incoherence, [13] proposed a review dedicated to the interpretation of the convective heat transfer of nanofluids and concluded that a nanofluid could be considered a homogeneous fluid with altered properties, since these properties effectively belong to the nanofluid.

With the aim of help on the clarification of the effects that nanoparticles have on the CHTC of liquid coolants, researchers from Instituto Superior Técnico conceived and produced an experimental setup where an Al_2O_3-isopropanol nanofluid was tested. The selection of such nanofluid, which they report to be stable and Newtonian under all the tested working conditions, intends to enlarge the options of non-water based nanofluids available on the literature [14]. The experimental setup consisted in a closed duct circuit inside which the nanofluid flows, being then submitted to a constant heat flux supplied at the test section, a 2.4m long circular tube, horizontally placed and with an internal diameter of 3.5mm. For both laminar and turbulent fully developed flow conditions, the tests consisted on the evaluation of friction factor and CHTC, measuring the pressure drop and wall and fluid temperatures for samples of nanofluid at several inlet temperatures, nanoparticle concentrations, mass flow rates and heat fluxes, in stationary conditions [14].

The present work appears as a complement of [14], providing a numerical tool developed using the CFD code ANSYS-Fluent® based on the single-phase conventional approach, with the main goal of predicting the experimental measurements of CHTC and friction factor within a small range of error. Associated to that is, in fact, a verification of the hypothesis of homogeneous fluid suggested by [13], once thermal properties are available for the nanofluid. Moreover, a parametric study is proposed, in which we will infer about the influence of each controlling parameter on the thermal performance of the nanofluid, concluding with the examination of the influence of the constant Re comparison basis on the final results interpretation.

2. Mathematical modeling

2.1. Governing equations for fluid flow with heat transfer

[15] proposed a model to rule a dilute and Newtonian nanofluid flow in which he presented an extra transport equation for the nanoparticle concentration. Since [13] suggests that for dilute mixtures the mechanisms supposedly responsible for disorganized nanoparticle movement within the flow are small compared with traditional diffusion mechanisms, neglecting them is perfectly reasonable. Moreover, during our simulations we intend to keep constant the particle concentration by assuming a perfect homogeneity inside the flow, which implies no need of transport equation for nanoparticles. The resulting governing equations are then the

same as for pure fluid, but with effective properties, meaning that for an incompressible and Newtonian fluid flow we have [16]

$$\nabla \cdot \mathbf{u} = \mathbf{0} \tag{1a}$$

$$\rho \frac{D\mathbf{u}}{Dt} = \rho \mathbf{g} - \nabla p + \nabla \cdot \left[\mu \left(\nabla \mathbf{u} + (\nabla \mathbf{u})^T\right)\right] \tag{1b}$$

$$\rho c_p \frac{DT}{Dt} = \nabla \cdot (k \nabla T) + \Phi \tag{1c}$$

where $\mathbf{u}$ is the velocity vector, ρ the density, $\mathbf{g}$ the gravity acceleration vector, p the pressure, μ the dynamic viscosity, c_p the specific heat, k the thermal conductivity, T the temperature and Φ the viscous dissipation fuction.

The system of equations 1 represents the continuity, Navier-Stokes and energy equations, respectively.

2.2. Basic notions on internal flows

The mass flow rate, $\dot{m}$, from which is possible to compute the mean flow velocity, u_m, is given by [17]

$$\dot{m} = \rho u_m A_c = \int_{A_c} \rho u \, dA_c \tag{2}$$

in which A_c means the cross-sectional area. This flow, in fully developed conditions, has the particularity of being one of the known analytical solutions of equations 1b, granting an analytical expression for the velocity profile. Therefore, it is possible to compute the Darcy friction factor directly from [17]

$$f = \frac{64}{Re_D} \tag{3}$$

where $Re_D = \rho u_m D/\mu$. This factor is a non-dimensional parameter of extremely practical importance since, when known, it allows the computation of the pressure drop of the flow, Δp, as [17]

$$\Delta p = \int_{x_1}^{x_2} f \frac{\rho u_m^2}{2D} \, dx \tag{4}$$

For turbulent flow there is no discovered solutions of the equations 1b, so f was experimentally measured and plotted in the Moody diagram, which gave rise to the implicit Colebrook equation [17]

$$\frac{1}{\sqrt{f}} = -2 \log \left(\frac{e/D}{3.7} + \frac{2.51}{Re_D \sqrt{f}} \right) \tag{5}$$

Similarly to the mean velocity, appears the mean temperature, T_m, equal to [17]

$$T_m = \frac{\int_{A_c} \rho c_p u T \, dA_c}{\dot{m} c_p} \tag{6}$$

It is a temperature that multiplied by the mass flow rate and the specific heat gives the rate of sensible energy carried by the fluid and its importance in internal flows is undeniable, since it allows the direct use of the Newton's cooling law and consequent estimation of the heat transfer coefficient, h, as [17]

$$q'' = h(T_s - T_m) \tag{7}$$

in which T_s means the surface temperature.

Even though h is the more important quantity in convection problems, its estimation process is usually preceded by the Nu computation, for which theoretical and semi-empirical equations are developed. This approach allows a cleaner calculation, since it eliminates a great number of variables influencing h. For this flow in laminar conditions, the correlation for $Nu_D = hD/k_f$ is given by [18]

$$Nu_D = \begin{cases} 1.302 x_*^{-1/3} - 1 \\ \text{for } x_* \leq 0.00005 \\ 1.302 x_*^{-1/3} - 0.5 \\ \text{for } 0.00005 < x_* \leq 0.0015 \\ 4.364 + 8.68(1000 x_*)^{-0.506} \exp(-41 x_*) \\ \text{for } x_* > 0.0015 \end{cases} \tag{8}$$

where $x_* = (x/D)/(Re_D Pr)$. Regarding turbulent flow, one of the possibilities to compute Nu is using the Gnielinski equation [18]

$$Nu_D = \frac{(f/8)(Re_D - 1000)Pr}{1 + 12.7(f/8)^{1/2}(Pr^{2/3} - 1)} \tag{9}$$

2.3. Modeling turbulence

The totally chaotic movement powered by turbulence produces a set of fluctuations that makes an instantaneous measurement of a flow quantity an extremely complex signal. So, it is usual to decompose all instantaneous flow quantities into their mean value, plus a fluctuating component, like

$$\theta(\mathbf{r}, t) = \Theta(\mathbf{r}) + \theta'(\mathbf{r}, t) \tag{10}$$

where θ represents a scalar or vector quantity. This is called the Reynolds decomposition and if we employ this modification to velocity, temperature and pressure instantaneous fields and replace them into equations 1, we end up with the Reynolds-averaged Navier-Stokes (RANS) equations and Reynolds-averaged energy equation, equal to [16]

$$\nabla \cdot \mathbf{U} = 0 \tag{11a}$$

$$\rho \frac{D\mathbf{U}}{Dt} = \rho \mathbf{g} - \nabla P + \nabla \cdot \left[\mu \left(\nabla \mathbf{U} + (\nabla \mathbf{U})^T\right) - \rho \overline{\mathbf{u}'\mathbf{u}'}\right] \tag{11b}$$

$$\rho \frac{D\mathcal{T}}{Dt} = \nabla \cdot \left(\frac{k}{c_p} \nabla \mathcal{T} - \rho \overline{\mathbf{u}' T'} \right) + \frac{\Phi}{c_p} \tag{11c}$$

The appearance in RANS equations of the Reynolds stress tensor, $\boldsymbol{\tau}^R = -\rho \overline{\mathbf{u}'\mathbf{u}'}$, totally unknown a priori, powered the advent of the turbulence models, empirical models responsible to estimate them. Due to our simple geometry and incompressible flow, any two-equation model should

produce satisfactory results. The choice ended up to be the SST $\kappa-\omega$ since it has no restrictions while applied in the near-wall zone.

2.4. Modeling thermophysical properties

For the nanofluid in question, the measured values for density can be adequately predicted employing the following equation [19]

$$\rho_{nf} = 808.7697 - 0.9508T + 6.4576\omega \tag{12}$$

where ρ_{nf} means the density in [kg/m^3], T the temperature in [^{o}C] and ω the particle mass fraction in [%].

Dynamic viscosity exhibit different non-linear behavior with T and ω and, contrarily to density, fitting a single equation to predict its values within the entire variation range of the parameters was not possible. For that reason, an equation for each ω [%] studied was proposed, in the form of [19]

$$\mu_{nf} = \begin{cases} (a+bT)^{-1}, & \omega = \{0; 0.387; 0.992; 3.12\} \\ (a-b/T^2)^{-1}, & \omega = \{4.71\} \end{cases} \tag{13}$$

in which μ_{nf} is the dynamic viscosity in [Pa.s] and a and b are constants with values given in table 1.

Table 1: Coefficients for the dynamic viscosity model.

ω [%]	0	0.387	0.992	3.12	4.71
a	175.5004	126.2533	137.8122	142.4812	355.8237
b	12.9337	12.5972	11.2665	7.8454	36462.5170

The case of thermal conductivity is quite similar to density, since it was possible to express the influence of the two parameters into one single model equation. Such equation is then equal to [19]

$$k_{nf} = 0.09545 + 0.00128\omega + \frac{13.1182}{T} \tag{14}$$

where k_{nf} is expressed in [W/(m.K)], ω in [%] and T in [K].

Finally, the model for specific heat at constant pressure is quite different and requires more auxiliary math than the others. It is approximately given by [19]

$$c_{p,nf} = \frac{a + bT^2 + cT^4}{M_{mix}} \tag{15}$$

where $c_{p,nf}$ appears in [J/(kg.K)], T in [K], a, b, and c are constants and M_{mix} [kg/mol] is the mixture molar mass equal to

$$M_{mix} = M_{bf}(1-y) + M_{np}y \tag{16}$$

with $M_{bf} = 0.060095$ and $M_{np} = 0.101961$ [kg/mol] being the substances' molar mass and y the particle molar fraction, given by

$$y = \left[1 + \frac{M_{np}}{M_{bf}}\left(\frac{1}{\omega} - 1\right)\right]^{-1}, \quad y > 0 \tag{17}$$

Note that in equation 17, ω appears in [kg/kg] to generate y in [mol/mol]. Constants a, b, and c are computed through the following set of equations, this time with y being used in [%].

$$a = 105.93 - 0.532y \tag{18a}$$

$$b = -1.43 \times 10^{-4} - 4.01 \times 10^{-6}y \tag{18b}$$

$$c = 7.89 \times 10^{-9} + 1.1 \times 10^{-11}y \tag{18c}$$

3. Numerical investigation

3.1. Finite volume method

Finite volume method (FVM) is a numerical technique widely used in CFD problems. It consists in the division of the computational domain into several aggregated control volumes (CVs), containing each one a grid node, for which a transport equation is integrated over the CV boundaries. This procedure creates an integral balance algebraic equation for each CV that replicated to the remaining CVs produces a coupled system of algebraic equations whose solution is the dependent variable value in each grid point.

The discretization process requires some approximations when computing the CV face values needed for fluxes' computation. If the derivatives of the diffusive term are well approximated assuming a linear variation between the two surrounding node values, the convective term requires a discretization scheme to compute the face values with weighted contributions from the surrounding nodes. Fluent® has available a second order upwind scheme (if unbounded is equivalent to FROOM in [16]) which reveals to be the most suited option since it ensures a second order error reduction without requiring a high computational effort [20].

Once selected the discretization scheme, it is possible to write an algebraic equation for each CV and finally build the system of discretized equations. For a scalar conserved quantity, θ, the generic discretization equation is equal to [16]

$$a_P\theta_P = \sum_{nb} a_{nb}\theta_{nb} + b \tag{19}$$

in which P represents the central node, nb the neighboring nodes, a_i the coefficients of the discrete equations (available in [16] for FROOM scheme) and b the independent term.

Such procedure allows the numerical solution of scalar transport equations, like equation 1c. On the other hand, the numerical solution of the Navier-Stokes equations requires a more complex procedure due to the pressure-velocity coupling. SIMPLE algorithm is an iterative technique especially designed to simultaneously find the velocity and pressure fields of the flow, but its convergence rate might be slow in some occasions. Taking that in mind, the segregated solver of Fluent® provides

an improved version - called SIMPLEC - which accelerates the convergence of the algorithm, reason why it will be used instead of SIMPLE when solving the Navier-Stokes and continuity equations [20].

The resulting systems of discrete equations for each flow variable are effectively solved in Fluent® using the iterative Gauss-Seidel method following an Algebraic Multigrid approach.

3.2. Boundary conditions

For laminar flow, at the inlet, the temperature field is considered constant and the flow fully developed, with a velocity profile described by [17]

$$\frac{u}{u_m} = 2\left[1 - \left(\frac{r}{R}\right)^2\right] \tag{20}$$

At the outlet, a pressure-outlet condition was considered, simulating a flow exit at atmospheric pressure. For the stationary tube wall, a no-slip condition was employed and a constant heat flux was defined. Finally, the axisymmetric character of our geometry allowed to define a symmetry condition along the symmetry axis. This last one is of great importance, since it allowed a reduction from a 3D geometry to a 2D flow sheet.

In turbulent case, equation 20 is no longer valid, being the fully developed flow conditions approximated by [21]

$$\frac{U}{U_{max}} = \left(1 - \frac{r}{R}\right)^n \tag{21}$$

where $n = 1/7$ and U_{max} is given by [21]

$$\frac{U_{avg}}{U_{max}} = \frac{2}{(n+1)(n+2)} \tag{22}$$

The turbulence model adds two extra transport equations that also need boundary conditions. For the inlet estimations of κ and ω, the procedure described in [22] based on the turbulence intensity, I, and on the hydraulic diameter was adopted. To the user, no more modifications are required and the remaining treatment for the laminar case remains valid for turbulent flow conditions.

3.3. Mesh independence study

The mesh has a strong influence on the solution process, reason why one should investigate when the results become independent of it. The 2D geometry allowed the use of a Cartesian structured mesh and this refinement process will only test meshes differing in the number of radial and axial CVs.

Independent meshes will be used for laminar and turbulent flow regimes due to the near-wall flow, requiring separate independence tests. Controlling conditions are presented in table 2 and the convergence criteria, adopted during the entire work, is the continuity's scaled residual inferior to 10^{-8} or

Table 2: Conditions adopted in the mesh convergence study.

Reg.	T_{in} [^oC]	$\dot{m}$ [kg/s]	q'' [W/m^2]	ω [%]	u/U	I [%]
Lam.	15	0.00767	1000	0	Parabolic	-
Turb.	15	0.0767	10000	0	Constant	5

κ's and ω's smaller than 10^{-7}. The grid selected is the one where the improvement in solution accuracy does not justify the extra time consumed.

For the laminar case, seven grids were contemplated where both temperature and axial velocity were tracked at $x = L/2$ and $r = 0$. From grid 1 to 5, the refinement was attained by doubling the number of CVs in both directions, until 3860×80 (n°CVx × n°CVr), being then grids 6 and 7 proposed with dimensions between grids 3 and 4. The refinement influence was better noticed in the axial velocity plot, illustrated in figure 1. Grid 6 was chosen since it produced almost equal results to grid 4 with a reduced number of CVs of 1440×30.

The key features evaluated for the turbulent case were h and the skin friction coefficient, C_f, equal to [17]

$$C_f = \frac{\tau_w}{\rho u_m^2/2} \tag{23}$$

where τ_w means the wall shear stress. Both temperature and velocity exhibit shaper slopes in the near-wall zone that need to be captured, and these two quantities represent a good indicator of their resolution and impact on computed quantities.

Due to this phenomenon, local refinement in the near-wall zone might be necessary, since equally spaced meshes probably do not capture with the necessary detail the gradients there. So, besides the refinement process, also a biased arrangement was proposed to be compared with the structured one. Using the know-how acquired in laminar case, only three grids were considered this time.

Results are available in figure 2. In (a), one can see C_f lines totally converged for biased meshes, proving the failure of an equally spaced mesh with the same number of CVs in capture the velocity gra-

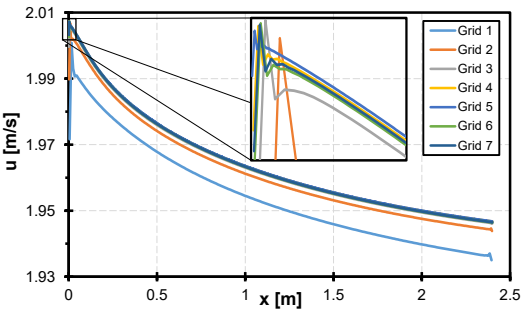

Figure 1: Velocity axial evolution at $r = 0$ for mesh independence study in laminar flow conditions.

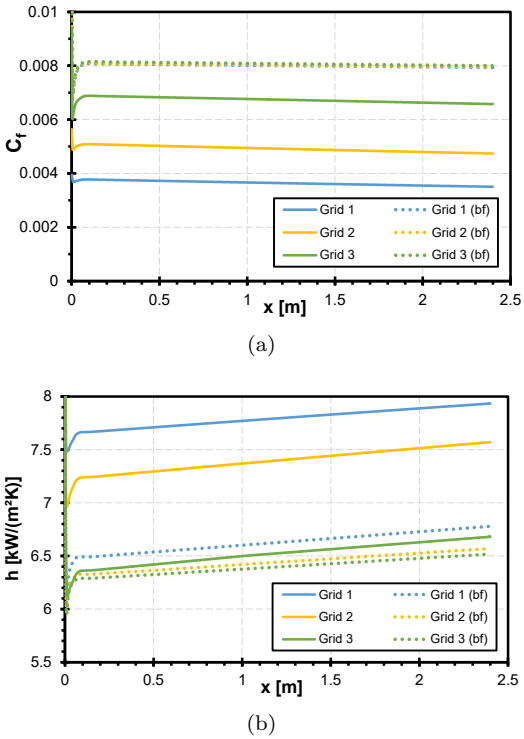

Figure 2: Axial evolution of (a) C_f and (b) h for mesh independence study in turbulent flow conditions.

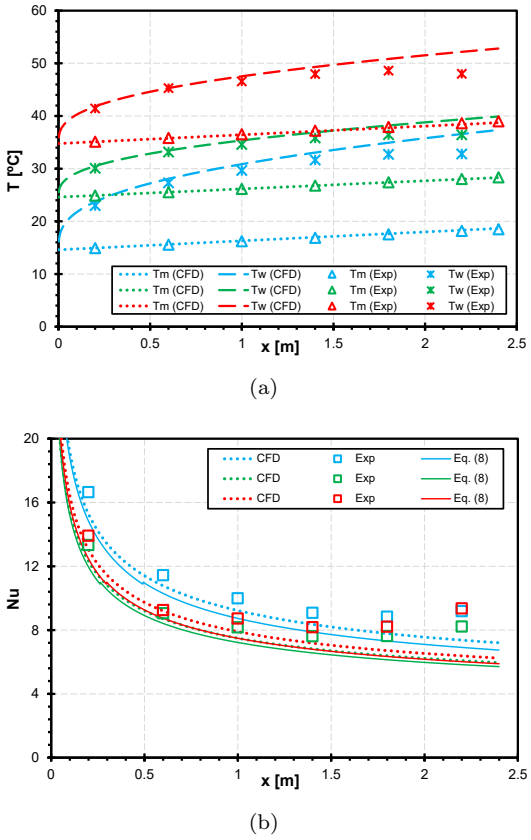

Figure 3: Isopropanol laminar predictions. (a) axial evolution of T_m and T_w and (b) axial evolution of Nu. Conditions $\Rightarrow$ $T_{in} = 14.6^oC$ (Blue) • $T_{in} = 24.6^oC$ (Green) • $T_{in} = 34.8^oC$ (Red).

dient with the desired detail. Similarly, (b) shows clear improvements from using a biased mesh in h computation and the small difference between the results from biased grids 2 and 3 indicates that biased grid 2, whose dimensions are 1920×40 and the bias factor is 15, is the most indicated one for turbulent simulations.

3.4. Model validation

This validation procedure intends to estimate the accuracy of the model by comparing measurements of the base fluid with their predictions and with theory, whenever possible. Thus, Nu, T_m and wall temperature, T_w, were tracked in non-isothermal tests, while f was the object of interest of isothermal replications.

For laminar flow conditions, figure 3 shows that for T_m experiments match perfectly the CFD line for each one of the studied inlet temperatures, although for T_w the agreement is very good up to $x = 1.4m$, loosing this trend in the last two points. Based on the theory, we expect a continuous axial increase of T_w which is not verified, for instance, in the $T_{in} \approx 35^oC$ case, reason why we relate this erratic trend to experimental errors. In terms of Nu, the agreement between theory, predictions and experiments is very good up to the fourth experimental point only, reflecting from there on the influence of the unexpected ΔT presented in figure 3 (a). Only 15% difference was found between experimental and theory values, confirming the good performance of the model for laminar simulations.

A similar study was conducted for turbulent regime and the results are given in figure 4. Both T_m and T_w were axially matched against measurements and Nu compared with experiments and equation 9 with f computed via equation 5. Again, predictions and measurements for T_m exhibit a better agreement than for T_w. Still, the trends of evolution are very close and totally acceptable.

In terms of Nu, the agreement between predictions and experiments can be considered very good whenever the numerical and experimental ΔT are very close, but any small difference in ΔT is highly amplified in terms of Nu. This is the main explanation for the observed results, since when no difference was noted on measured and predicted ΔT, experimental and computational Nu agree very well. Even though, and neglecting the last two experimental points, all the local predicted Nu are within 20% of the measured ones.

On the other hand, the Gnielinski equation was not able to correctly predict the local Nu. Such behavior has already been noticed in [7] and [9], so we accept it as expected. However, slopes of predic-

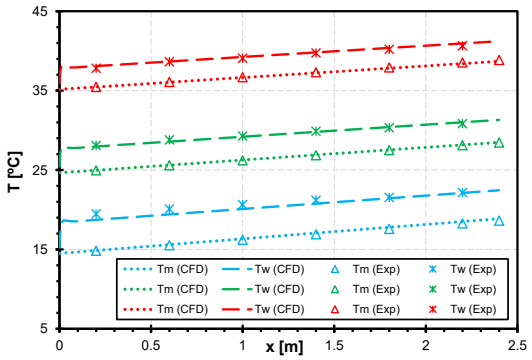

(a)

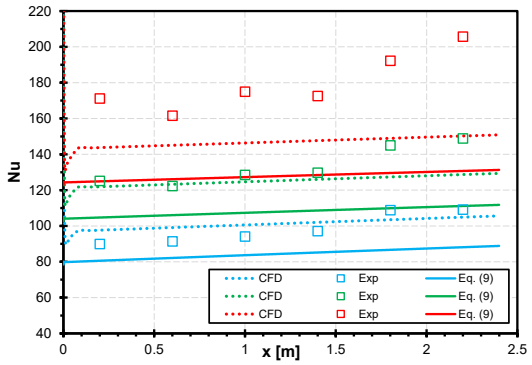

(b)

Figure 4: Isopropanol turbulent predictions. (a) axial evolution of T_m and T_w and (b) axial evolution of Nu. Conditions $\Rightarrow$ $T_{in} = 15.3^oC$ (Blue) • $T_{in} = 25.8^oC$ (Green) • $T_{in} = 35.1^oC$ (Red).

tions and Gnielinski lines are the same, supporting the rising trend of Nu and confirming the presence of small errors in temperature measurements.

Predictions and measurements for f in laminar and turbulent regimes, for the three considered inlet temperatures, are available in figure 5. There, they are compared against equations 3 and 5, this last one considering a roughness of 3 μm used in all the turbulent simulations performed [14]. For laminar

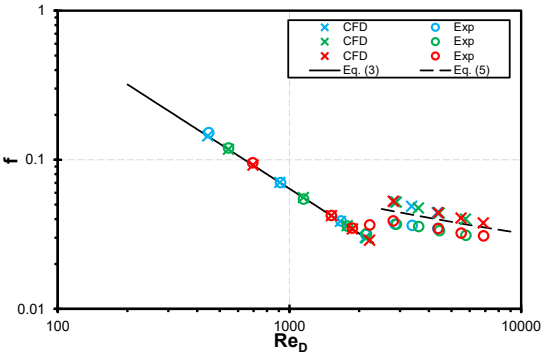

Figure 5: Isopropanol friction factor for laminar and turbulent regime. Conditions $\Rightarrow$ $T_{in} = 15^oC$ (Blue) • $T_{in} = 25^oC$ (Green) • $T_{in} = 35^oC$ (Red).

conditions, the agreement is almost perfect until $Re \approx 2150$, the value identified as the onset of transition to turbulent flow [14]. When turbulence is present, predictions at low Re are substantially superior than measured values and also than Colebrook equation, meaning a possible overestimation of the Δp effectively developed that becomes smaller as Re increases. As to us, it reveals the inferior performance of turbulence models in turbulence developing conditions.

4. Results and discussion

4.1. Predictions vs. experiments

Several cases like those from figures 3 and 4, this time regarding the nanofluid loaded at several particle concentrations, were numerically simulated in order to evaluate how accurately the model predicts the thermal and hydrodynamic characteristics of the nanofluid.

The average heat transfer coefficient, $\overline{h}$, given by

$$\overline{h} = \frac{1}{A_s}\int_{A_s} h dA_s \tag{24}$$

was the parameter chosen to quantify the thermal performance of the nanofluid and a direct comparison between the experimental and predicted $\overline{h}$ can be seen in figure 6.

Similarly to validation tests, laminar case shows a very good agreement among predictions and measurements, considering that only in four cases the error exceeds 10%. The reason for such discrepancy is unclear, apart from computational/experimental errors, once buoyancy effects were considered in [14] and revealed to be insignificant.

For turbulent flow the error magnitude involved is higher, especially for $T_{in} = 35^oC$, but only five cases exhibit errors over 20%. An increased growing rate of the experimental data over predictions, for higher $\overline{h}$ (consequence of higher $\dot{m}$ and q''), was noticed mainly for larger ω and the model was incapable to reproduce it. However, the good agreement exhibited for most cases with inlet temperatures of 15^oC and 25^oC make us wonder about what physical reason stands behind the large differences found for 35^oC, besides experimental errors.

Numerical results for f were gathered and compared with experimental measurements and the theoretical laws 3 and 5, as illustrated in figure 7. For laminar regime, in line with the previous tests already seen, the plot shows excellent agreement between theoretical, experimental and numerical data for the entire range of laminar Re.

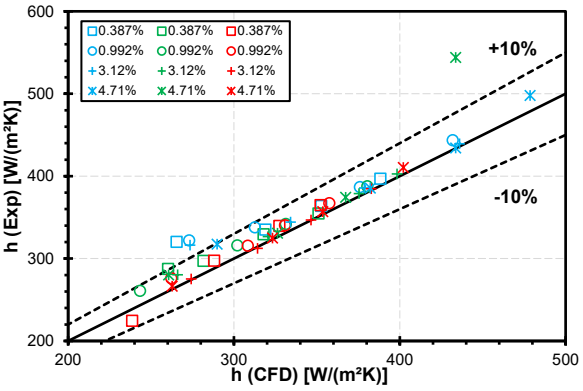

(a)

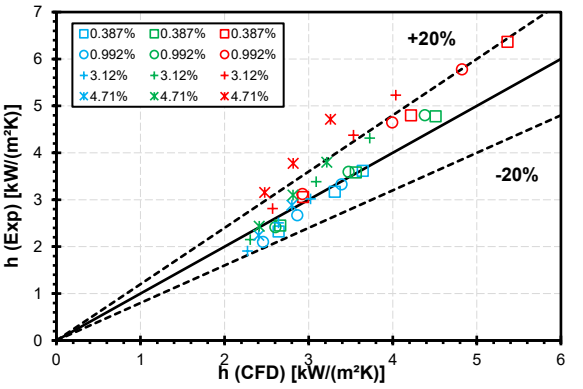

(b)

Figure 6: Comparison between numerical and experimental average heat transfer coefficients for (a) laminar regime and (b) turbulent regime. Blue data - $T_{in} = 15C$; Green data - $T_{in} = 25C$; Red data - $T_{in} = 35C$.

With respect to turbulent flow, not much can be added to what was already concluded when base fluid was investigated for validation purposes. Nevertheless, experimental data is always below predictions and Colebrook line, indicating a possible Δp overestimation even for larger Re than what really happens.

No influence of temperature or particle addition was noted in the numerical results for f, corroborating the experimental verification of Newtonian behavior for the Al_2O_3-isopropanol nanofluid.

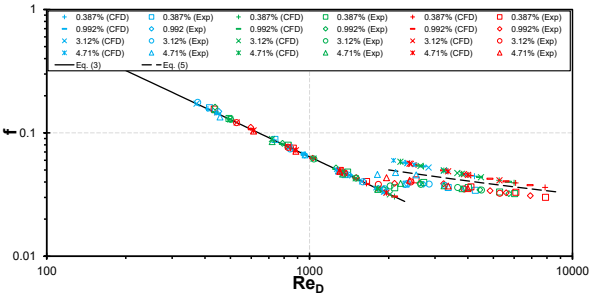

Figure 7: Al_2O_3-isopropanol friction factor predictions and experiments. Blue data - $T_{in} = 15^oC$; Green data - $T_{in} = 25^oC$; Red data - $T_{in} = 35^oC$.

4.2. Parametric analysis

This parametric analysis allow us to study the individual influence that mass flow rate, temperature and particle concentration has on the thermal performance of the nanofluid. Results contemplating both laminar and turbulent flow regimes are available in figure 8 and simulations were performed keeping a constant heat flux for each flow regime.

Figure 8 (a) clearly shows that $\overline{h}$ increases with $\dot{m}$. It makes sense, since mass flow rate powers fluid's bulk motion, a basic request of forced convection to exist. Also a higher T_{in} enhances $\overline{h}$, for a fixed $\dot{m}$ and q''. We attribute this increase to the c_p augmentation together with a ρ reduction due to the greater temperatures, which allows the fluid to absorb more energy per ^{o}C raised and accelerate by continuity, respectively.

The lack of improvement powered by nanoparticles addition is also curious. With exception of $T_{in} = 15^oC$ and $\omega = 4.71\%$ which claims some attention with its nearly 3% increase respectively to pure fluid, the heat transfer enhancement is almost unnoticed. This means that, when $\dot{m}$ is maintained, the k improvement given by nanoparticles is not enough to largely overcome the adverse contributions of ρ intensification and c_p decrease.

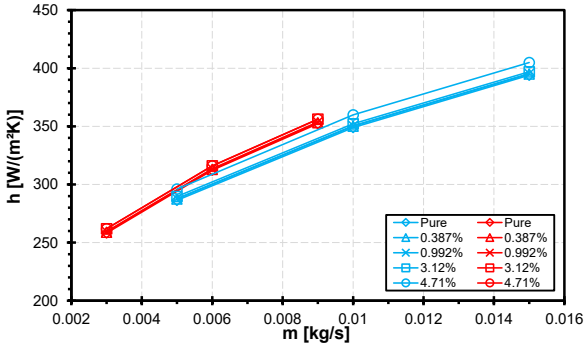

(a)

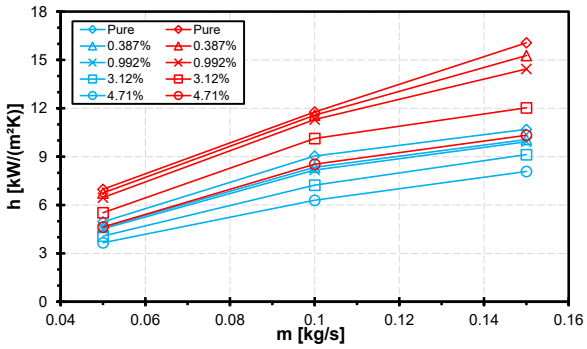

(b)

Figure 8: Influence of mass flow rate on average heat transfer coefficient for (a) laminar flow ($q'' = 1kW/m^2$) and (b) turbulent flow ($q'' = 10kW/m^2$). Blue data - $T_{in} = 15^oC$; Red data - $T_{in} = 35^oC$.

In spite of the distinct supporting mechanisms, figure 8 (b) demonstrates that the influence of $\dot{m}$ and T_{in} on $\overline{h}$ under the presence of turbulence is in line with laminar results. Turbulent transport has more importance on flow dynamics than properties variation and motivated a closer look on turbulent quantities when trying to find a reason to the $\overline{h}$ decrease with particles addition, which could reach 30% respectively to base fluid alone.

Since turbulent kinetic energy dissipation rate, ε, is directly related to turbulence production, it was investigated and an interesting correlation was found, showing that to the highest $\overline{h}$ was associated the largest ε. As ε is directly proportional to viscosity and strain rate intensity, we noticed that this $\overline{h}$ improvement came from a sharper velocity gradients within the turbulent boundary layer, since temperature promotes ε but reduces viscosity. So, the more turbulence produced, the better the thermal performance and, while temperature promotes this phenomenon, the addition of nanoparticles has a negative contribution on it. This conclusion is corroborated by the reduced degree of turbulence reported by [14] regarding the nanoparticles effect on $\overline{h}$ in turbulent flow conditions.

The reported observations agree qualitatively well with the data presented in [14] regarding the $\dot{m}c_p$ comparison basis.

4.3. Influence of constant Re comparison basis

The same data is now presented in a constant Re comparison basis, in order to investigate its influence on the results interpretation. This is the most used comparison basis in the literature but it completely ignores the effect of nanoparticles on the thermal properties. An equal Re simply ensures the same ratio of inertia to viscous forces and not the same dynamic conditions, so a viscosity variation imposed by exterior factors will imply a velocity change to keep the same force ratio, leading us to a comparison between two totally distinct dynamics. This is what supports the statements of [3] about the inviability of using Re as comparison basis.

Data for laminar flow is available in figure 9 (a), and comparing it with that presented before for mass flow rate comparison basis, some differences are clearly noticed. The first one is that $\overline{h}$ is enhanced by a temperature reduction. This happens because μ is reduced by temperature and keep the same Re will only be achieved thanks to a $\dot{m}$ reduction. This $\overline{h}$ enhancement is about 10 to 14% in comparison with the base fluid but is, in fact, a consequence of the higher $\dot{m}$ considered for $T_{in} = 15^{o}C$ rather than a temperature reduction.

For a constant T and $\dot{m}$, Re is significantly reduced as long as ω increases from 0% to 4.71%. What succeeds is that such reduction allows a separation of the ω-constant lines, reflecting a supposed improvement of $\overline{h}$. For $\omega = 4.71\%$ and considering the same Re, an enhancement superior to 20% in $\overline{h}$ was verified when compared to the base fluid. This suggests that a nanofluid is prone to have a superior thermal performance as long as it contains more nanoparticles, which we already proved to be true, but in totally different proportions. This qualitative improvement tendency agrees with the majority of the laminar investigations given in section 1, where both Re and ω were identified as sources of improvement for $\overline{h}$ for several types of nanofluids, and also with [14], confirming what has been presented and discussed until now.

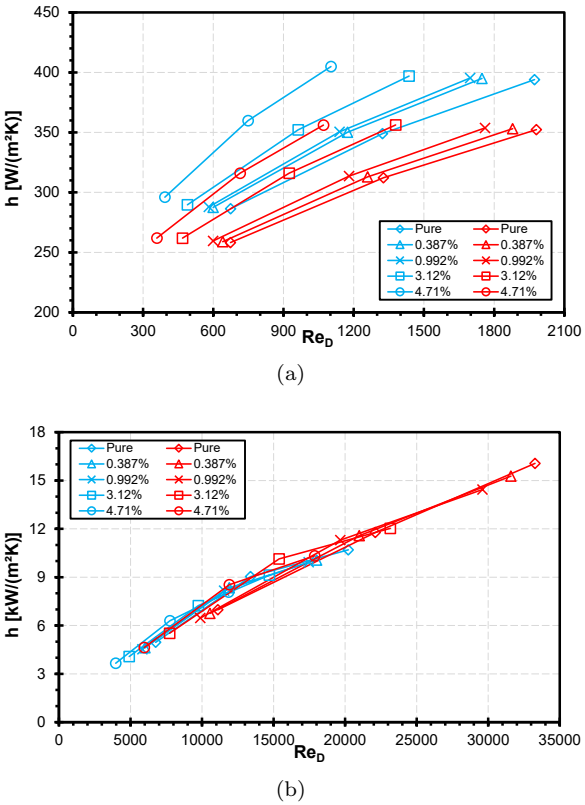

Figure 9: Average heat transfer coefficient compared under constant Re basis for (a) laminar flow ($q'' = 1kW/m^2$) and (b) turbulent flow ($q'' = 10kW/m^2$). Blue data - $T_{in} = 15^{o}C$; Red data - $T_{in} = 35^{o}C$.

For turbulent flow conditions, constant Re basis has revealed a curious insensitivity of the $\overline{h}$ on temperature and particle concentration variations, clearly contrasting with the decrease of $\overline{h}$ powered by particles addition and the favorable effect of temperature, observed in figure 8 (b).

5. Conclusions

In conclusion, the model performs well while predicting the heat transfer conditions of a laminar Al_2O_3-isopropanol flow, as demonstrated by the good match between predictions and experimen-

tal data. Based on that, we can confirm that this nanofluid follows very well the hypothesis of being correctly represented as a homogeneous fluid with altered properties. Predictions for turbulent flow revealed an inferior degree of agreement in relation to laminar case, still the differences in the majority of simulations were kept within an acceptable error level, validating the hypothesis when turbulence is present as well.

Improvements in the CHTC directly related to Al_2O_3 nanoparticles addition were only found in laminar flow conditions. However, those percentages are quite small and possibly do not justify their use replacing the base fluid alone, since their manufacture requires an additional economical effort and they might suffer from long stability problems. Even though, if these are considered minor problems, as well as the extra pumping power, it is possible to attain a better performance using this nanofluid in laminar forced convection applications. Nevertheless, one should not blindly trust on the quantification of the enhancements resultant from a constant Re comparison basis, since the realities compared are not really the same. No advantage was seen from the use of Al_2O_3-isopropanol nanofluids in turbulent flow conditions.

References

[1] World Energy Outlook 2017. International Energy Agency. `https://www.iea.org/weo2017/#section-6`, last access in October 2018.

[2] W. Yu, D. M. France, J. L. Routbort, and S. U. S. Choi. Review and comparison of nanofluid thermal conductivity and heat transfer enhancements. *Heat Transfer Engineering*, 29(5):432460, 2008. doi: 10.1080/01457630701850851.

[3] W. Yu, D. M. France, E. V. Timofeeva, D. Singh, and J. L. Routbort. Comparative review of turbulent heat transfer of nanofluids. *International Journal of Heat and Mass Transfer*, 55:5380–5396, October 2012. doi: 10.1016/j.ijheatmasstransfer.2012.06.034.

[4] W. Y. Lai, B. Duculescu, P. E. Phelan, and R. Prasher. Convective heat transfer with nanofluids in a single 1.02-mm tube. In *Proceedings of the ASME International Mechanical Engineering Congress and Exposition*, 2006.

[5] K. S. Hwang, S. P. Jang, and S. U. S. Choi. Flow and convective heat transfer characteristics of water-based Al_2O_3 nanofluids in fully developed laminar flow regime. *International Journal of Heat and Mass Transfer*, 52:193–199, January 2009. doi: 10.1016/j.ijheatmasstransfer.2008.06.032.

[6] D. Kim, Y. Kwon, Y. Cho, C. Li, S. Cheong, Y. Hwang, J. Lee, D. Hong, and S. Moon. Convective heat transfer characteristics of nanofluids under laminar and turbulent flow conditions. *Current Applied Physics*, 9:119–123, 2009. doi:10.1016/j.cap.2008.12.047.

[7] R. Martnez-Cuenca, R. Mondragn, L. Hernndez, C. Segarra, J. C. Jarque, T. Hibiki, and J. E. Juli. Forced-convective heat-transfer coefficient and pressure drop of water-based nanofluids in a horizontal pipe. *Applied Thermal Engineering*, 98:841–849, April 2016. doi: 10.1016/j.applthermaleng.2015.11.050.

[8] W. Williams, J. Buongiorno, and L.-W. Hu. Experimental investigation of turbulent convective heat transfer and pressure loss of alumina/water and zirconia/water nanoparticle colloids (nanofluids) in horizontal tubes. *Journal of Heat Transfer*, 130(042412), April 2008. doi: 10.1115/1.2818775.

[9] P. K. Namburu, D. K. Das, K. M. Tanguturi, and R. S. Vajjha. Numerical study of turbulent flow and heat transfer characteristics of nanofluids considering variable properties. *International Journal of Thermal Sciences*, 48:290–302, 2009. doi: 10.1016/j.ijthermalsci.2008.01.001.

[10] V. Bianco, F. Chiacchio, O. Manca, and S. Nardini. Numerical investigation of nanofluids forced convection in circular tubes. *Applied Thermal Engineering*, 29:3632–3642, July 2009. doi: 10.1016/j.applthermaleng.2009.06.019.

[11] G. Saha and M. C. Paul. Numerical analysis of the heat transfer behaviour of water based Al_2O_3 and TiO_2 nanofluids in a circular pipe under the turbulent flow condition. *International Communications in Heat and Mass Transfer*, 56:96–108, August 2014. doi: 10.1016/j.icheatmasstransfer.2014.06.008.

[12] Y. Xuan and W. Roetzel. Conceptions for heat transfer correlation of nanofluids. *International Journal of Heat and Mass Transfer*, 43:3701–3707, 2000. PII: S00 1 7-93 1 0(99)0 03 6 9- 5.

[13] M. Buschmann, R. Azizian, T. Kempe, J. Juli, R. Martnez-Cuenca, B. Sundn, Z. Wu, A. Seppl, and T. Ala-Nissila. Correct interpretation of nanofluid convective heat transfer. *International Journal of Thermal Sciences*, 129:504–531, July 2018. doi: 10.1016/j.ijthermalsci.2017.11.003.

[14] A. Nikulin, A. S. Moita, A. L. N. Moreira, S. M. S. Murshed, A. Huminic, Y. Grosu, A. Faik, J. Nieto-Maestre, and O. Khliyeva. Effect of Al_2O_3 nanoparticles on laminar, transient and turbulent flow of isopropyl alcohol. *International Journal of Heat and Mass Transfer*, 130:1032–1044, March 2019. doi: 10.1016/j.ijheatmasstransfer.2018.10.114.

[15] J. Buongiorno. Convective transport in nanofluids. *Journal of Heat Transfer*, 128, March 2006. doi: 10.1115/1.2150834.

[16] F. Moukalled, L. Mangani, and M. Darwish. *The Finite Volume Method in Computational Fluid Dynamics*. Springer, 2016. ISBN: 978-3-319-16873-9.

[17] T. L. Bergman, A. S. Lavine, F. P. Incropera, and D. P. Dewitt. *Fundamentals of Heat and Mass Transfer*. John Wiley & Sons, Inc., 7^{th} edition, 2011. ISBN: 978-0470-50197-9.

[18] A. Bejan. *Convection Heat Transfer*. John Wiley & Sons, Inc., 4^{th} edition, 2013. ISBN: 978-0-470-90037-6.

[19] A. Nikulin. Personal communication. 2019.

[20] *ANSYS Fluent Theory Guide, Release 18.0*. ANSYS, Inc., January 2017.

[21] F. M. White. *Fluid Mechanics*. McGraw-Hill Education, 8^{th} edition, 2016. ISBN: 978-0-07-339827-3.

[22] *ANSYS Fluent User's Guide, Release 18.1*. ANSYS, Inc., April 2017.